Available online at www.sciencedirect.com
ScienceDirect
Journal of Power Sources 174 (2007) 1218–1223
JOURNAL OF POWER SOURCES
www.elsevier.com/locate/jpowsour

Short communication

Structural and electrochemical properties of $Li_{0.44+x}Mn_{1-y}Ti_yO_2$ as a novel 4 V positive electrode material

Junji Awaka [a], Junji Akimoto [a,*], Hiroshi Hayakawa [a], Yasuhiko Takahashi [a], Norihito Kijima [a], Mitsuharu Tabuchi [b], Hikari Sakaebe [b], Kuniaki Tatsumi [b]

[a] *National Institute of Advanced Industrial Science and Technology (AIST), AIST Tsukuba Central 5, 1-1-1 Higashi, Tsukuba, Ibaraki 305-8565, Japan*
[b] *National Institute of Advanced Industrial Science and Technology (AIST), AIST Kansai, 1-8-31 Midorigaoka, Ikeda, Osaka 563-8577, Japan*

Available online 23 June 2007

Abstract

The specific capacity of $Li_{0.44}Mn_{1-y}Ti_yO_2$ ($0<y<0.22$) positive electrode materials has been improved by an additional lithium-insertion treatment in molten $LiNO_3$–LiOH salt at a low temperature. High-purity specimens of the lithium-inserted $Li_{0.44+x}Mn_{1-y}Ti_yO_2$ have been successfully prepared. We have conducted a systematic experimental study of the structural and electrochemical properties of these compounds. The inserted lithium content, x, in $Li_{0.44+x}Mn_{1-y}Ti_yO_2$ increases together with the substituted Ti content, y. The initial charge capacity increases from 130 mAh g^{-1} ($y=0$) to 145 mAh g^{-1} ($y=0.22$) for the $Li_{0.44+x}Mn_{1-y}Ti_yO_2$ compounds. The maximum discharge capacity that has been achieved is 180 mAh g^{-1} in the case of $Li_{0.72}Mn_{0.78}Ti_{0.22}O_2$ between 2.5 and 4.8 V with a fixed current density of 30 mA g^{-1} ($C/6$) at 30 °C. The discharge capacity at the 4 V plateau region (about 100 mAh g^{-1}) in the lithium-inserted $Li_{0.55}MnO_2$ has been improved to twice that in as-prepared $Li_{0.44}MnO_2$ (about 50 mAh g^{-1}). The structural differences between $Li_{0.44}MnO_2$ and $Li_{0.55}MnO_2$ are discussed based on XRD Rietveld analysis results.

Keywords: Lithium manganese oxide; $Li_{0.44}MnO_2$; Tunnel structure; Ion exchange; Lithium insertion; Electrochemical property

1. Introduction

Lithium manganese oxide, $Li_{0.44}MnO_2$, has been extensively investigated as a positive electrode material for secondary lithium batteries [1–5]. This compound can be prepared by a soft-chemical method using the corresponding sodium manganese oxide as the parent compound [1,2]. The crystal structure of $Li_{0.44}MnO_2$ [2] maintains the parent $Na_{0.44}MnO_2$-type tunnel structure [6,7], which differs from that of the well-known rocksalt-related lithium manganese oxides such as spinel-type $LiMn_2O_4$ and layered $LiMnO_2$. Hence, this compound does not undergo a conversion to spinel structure during normal cycling or upon heating below approximately 400 °C [4]. Unfortunately, the discharge voltage reported previously is about 3 V, and the discharge capacity between 3.6 and 2.5 V is about 95–100 mAh g^{-1} [1–4].

Recently, we investigated the preparation conditions by the molten-salt method and successfully improved the discharge/charge performance [5]. A novel 4 V plateau was observed in $Li_{0.44}MnO_2$ and in the titanium-substituted solid-solution compounds $Li_{0.44}Mn_{1-y}Ti_yO_2$ ($0<y<0.55$). A large discharge capacity (>150 mAh g^{-1}) was reported between 2.5 and 4.8 V for all the Li/$Li_{0.44}Mn_{1-y}Ti_yO_2$ cells [5]. Therefore, it is clearly confirmed that the $Li_{0.44}MnO_2$ material is interesting not only for its good cycle performance [4] but also for its high-voltage and high specific capacity [5]. However, the experimentally demonstrated capacity is still less than the theoretical capacity (193 mAh g^{-1}) from a structural viewpoint [4]; therefore, we are continuing with our attempts to improve the electrochemical performance. In the present study, a careful optimization of the ion-exchange conditions has been performed, and the specific capacity of $Li_{0.44}Mn_{1-y}Ti_yO_2$-type positive electrode materials has been improved by an additional lithium-insertion reaction in molten $LiNO_3$–LiOH at a low temperature.

2. Experimental

First, the precursor $Na_{0.44}Mn_{1-y}Ti_yO_2$ with $y=0$, 0.055, 0.11, and 0.22 was prepared in a method similar to that reported previously [5]. A mixture of Na_2CO_3, Mn_2O_3, and TiO_2 in the desired proportion was heated at 1000 °C in air. A starting

* Corresponding author. Tel.: +81 29 861 4408; fax: +81 29 861 9214.
E-mail address: j.akimoto@aist.go.jp (J. Akimoto).

0378-7753/$ – see front matter © 2007 Elsevier B.V. All rights reserved.
doi:10.1016/j.jpowsour.2007.06.042

ratio of Na/(Mn + Ti) = 0.5 was required to prevent the loss of the sodium component by volatilization at high temperature. The resultant specimens were reground, and the same temperature program sequences were repeated once again, respectively. In the case of the preparation of $Na_{0.44}MnO_2$ ($y = 0$), the mixture was heated at 900 °C because of the production of the $Na_{0.70}MnO_2$ phase at higher temperatures, as previously reported [5].

Sodium/lithium ion-exchange experiments were performed using a molten salt composed of a mixture of $LiNO_3$ and LiCl at 270–300 °C for 10 h in air. In the present study, a further lithium-insertion treatment was accomplished by heating as-prepared $Li_{0.44}Mn_{1-y}Ti_yO_2$ in molten $LiNO_3$–LiOH at 270–300 °C for 10 h in air. After heat treatment, the reaction mixture was washed with distilled water and ethanol, and then dried at room temperature. Hereafter, the samples obtained after the lithium-insertion treatments are denoted as $Li_{0.44+x}Mn_{1-y}Ti_yO_2$ ($0 < y < 0.22$).

The phase purity and crystal structure of the obtained samples were characterized by the X-ray powder diffraction (XRD) profiles measured with Cu Kα radiation using a Rigaku RINT2550V diffractometer (operating conditions: 40 kV, 200 mA) equipped with a curved graphite monochromator. The XRD data were collected for 1 s at each 0.02° step over a 2θ range from 5° to 120°. The computer program RIETAN-2000 was used for the Rietveld analysis [8].

The particle morphology and chemical composition were investigated by scanning electron microscopy-energy dispersive X-ray analysis (SEM-EDX, JEOL JSM-5400). The chemical analysis of the Li, Na, Mn, and Ti contents was carried out by inductively coupled plasma-atomic emission spectroscopy (ICP-AES) (Perkin Elmer, Inc., Optima 3000). The particle shape and average particle size were characterized by BET specific surface area measurement (Micromeritics FlowSorb-2300) and using a particle size analyzer (Microtrac), respectively.

Charge and discharge tests were performed at 30 °C using a positive electrode, which consisted of the sample (20 mg), acetylene black (5 mg), and polytetrafluoroethylene (PTFE) powder (0.5 mg) between 2.5 and 4.8 V against a Li-metal negative electrode at a fixed current density of 30 mA g^{-1}, which corresponds to the *C*/6 rate with respect to the ideal capacity. The electrochemical test cells were constructed with a stainless steel coin-type configuration. The separator was a microporous polypropylene sheet. A solution of 1 M $LiPF_6$ in a 50:50 mixture of ethylene carbonate (EC) and diethylcarbonate (DEC) by volume (Tomiyama Pure Chemical Industries, Ltd., battery grade) was used as the electrolyte. The cells were constructed in an argon-filled glove box.

3. Results and discussion

3.1. Synthesis

Fig. 1 shows the XRD patterns for the as-prepared $Na_{0.44}MnO_2$, ion-exchanged $Li_{0.44}MnO_2$, and lithium-inserted $Li_{0.55}MnO_2$ samples. All of the products were identified to be of single phase with the $Na_{0.44}MnO_2$-type structure, an orthorhombic crystal system, and space group *Pbam* [7]; this was confirmed

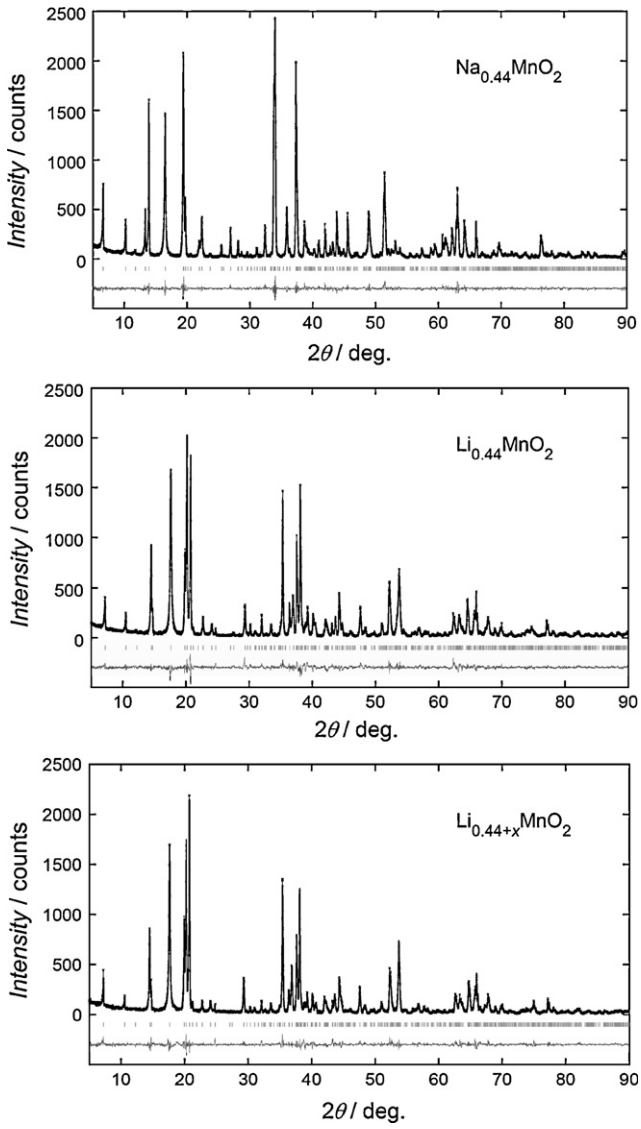

Fig. 1. Observed (plus marks), calculated (solid line), and difference (bottom) XRD patterns for $Na_{0.44}MnO_2$, $Li_{0.44}MnO_2$, and lithium-inserted $Li_{0.44+x}MnO_2$ ($x = 0.11$).

not only for the ion-exchange samples but also the lithium-inserted samples of the present study. Fig. 2 compares the typical SEM images obtained for the $Na_{0.44}MnO_2$, $Li_{0.44}MnO_2$, and the lithium-inserted $Li_{0.55}MnO_2$ samples. The particle morphology and size remained nearly unchanged after the molten-salt treatments. The average particle size (D50%) and the specific surface area were determined to be 6.40 μm and 1.7 m^2 g^{-1}, respectively, for the $Li_{0.44}MnO_2$ sample.

Table 1 lists the results of a chemical analysis of the $Li_{0.44+x}Mn_{1-y}Ti_yO_2$ samples by ICP-AES. As reported previously, the lithium content was in the range of 0.42–0.45 in the as-prepared $Li_{0.44}Mn_{1-y}Ti_yO_2$ samples [5]. On the other hand, the lithium content increased due to the lithium-insertion reaction using the $LiNO_3$–LiOH molten salt. This fact can be explained by the chemical lithiation of the $Li_{0.44}Mn_{1-y}Ti_yO_2$ samples performed using LiOH as a reducing agent. In addition, the lithium content, *x*, increased together with the Ti content, *y*,

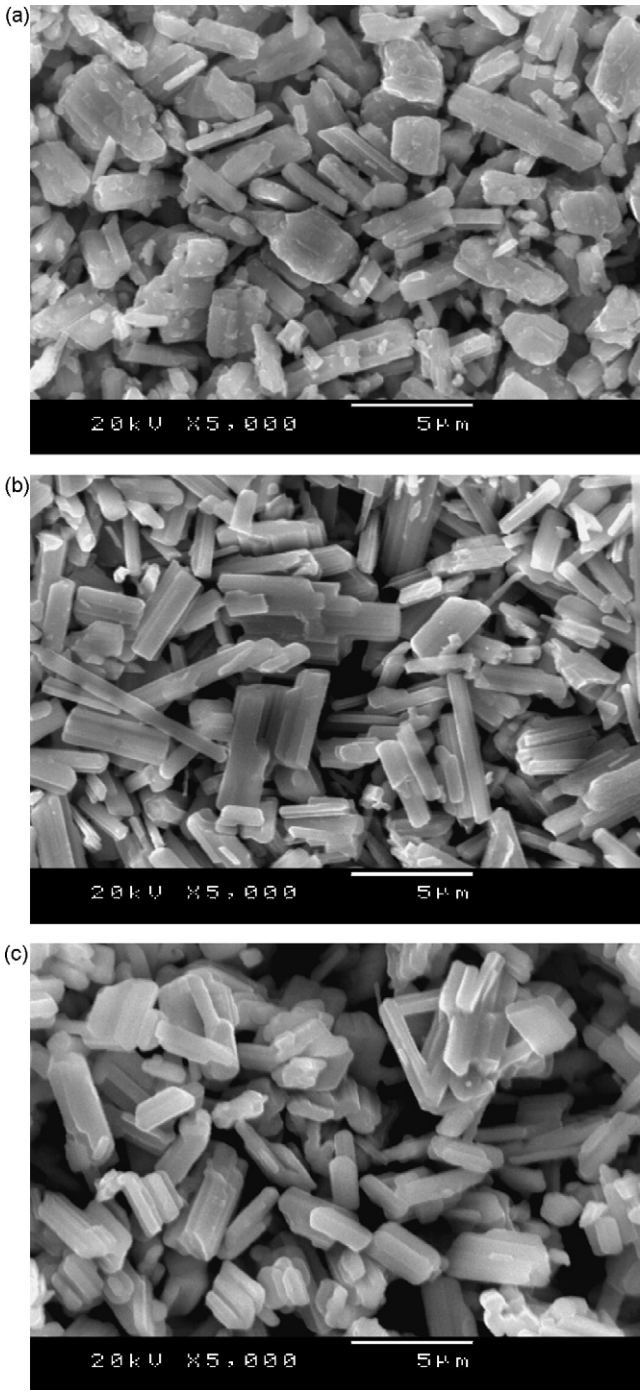

Fig. 2. SEM images of (a) $Na_{0.44}MnO_2$, (b) $Li_{0.44}MnO_2$, and (c) lithium-inserted $Li_{0.55}MnO_2$ samples.

Table 1
Chemical composition[a] of the products by ICP-AES analysis

Sample	Li	Na	Mn	Ti
$Li_{0.44+x}MnO_2$ ($y=0$)	0.55	<0.001	1	–
$Li_{0.44+x}Mn_{1-y}Ti_yO_2$ ($y=0.055$)	0.59	0.002	0.945	0.055
$Li_{0.44+x}Mn_{1-y}Ti_yO_2$ ($y=0.11$)	0.69	0.002	0.89	0.11
$Li_{0.44+x}Mn_{1-y}Ti_yO_2$ ($y=0.22$)	0.72	0.003	0.78	0.22

[a] The (Mn + Ti) content is fixed at 1.

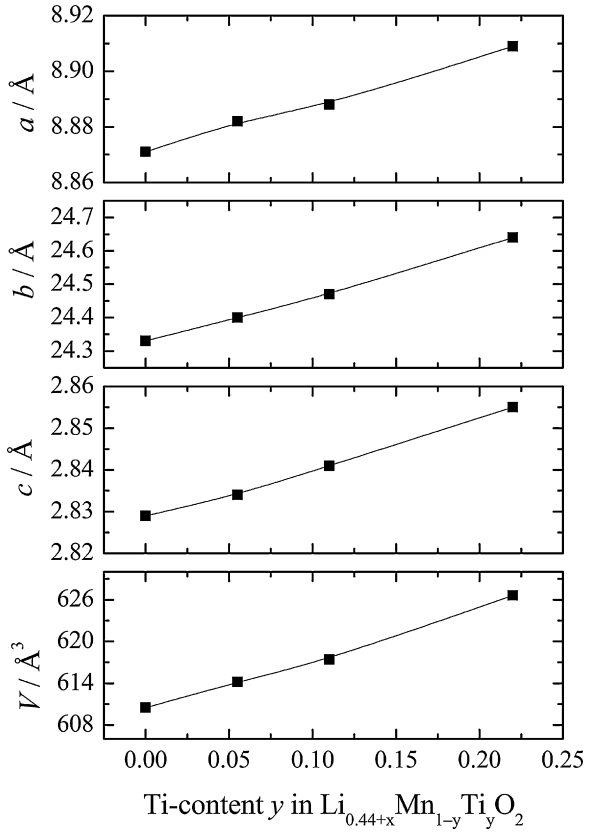

Fig. 3. Lattice parameters vs. Ti content in the $Li_{0.44+x}Mn_{1-y}Ti_yO_2$ samples.

in the present samples, as seen in Table 1. At the same time, the residual Na content increased with the Ti content in the $Li_{0.44+x}Mn_{1-y}Ti_yO_2$ samples. It should be noted that the Na content in the $Li_{0.55}MnO_2$ sample was less than 0.001, which is much smaller than that in the as-prepared $Li_{0.44}MnO_2$ sample, as reported previously [5].

3.2. Crystal structures

The lattice parameters for the present $Li_{0.44+x}Mn_{1-y}Ti_yO_2$ samples were refined using the XRD data (Fig. 1) with the least-squares method. Fig. 3 shows the lattice parameter versus the Ti content in the present samples. All of the lattice parameters gradually increased with the substituted Ti content from $y=0$ to $y=0.22$. The lattice parameters obey Vegard's law with an excellent agreement, where these experimental results depend linearly on the composition y. In addition, the a-axis lengths for these $Li_{0.44+x}Mn_{1-y}Ti_yO_2$ samples were apparently smaller than those for the as-prepared $Li_{0.44}Mn_{1-y}Ti_yO_2$ samples [4]. For example, the a-axis length for the present $Li_{0.44+x}Mn_{0.78}Ti_{0.22}O_2$ sample (8.909 Å) was smaller than that for the $Li_{0.44}Mn_{0.78}Ti_{0.22}O_2$ sample (8.964 Å) reported previously [4]. This difference can be explained by a local structural change after the lithium-insertion treatments, although the $Na_{0.44}MnO_2$-type framework structure remained unchanged, as can be seen in Fig. 1.

Fig. 4 shows the crystal structures of $Na_{0.44}MnO_2$, $Li_{0.44}MnO_2$, and $Li_{0.55}MnO_2$ determined by the Rietveld analysis. The lithium positions could not be refined in the present XRD

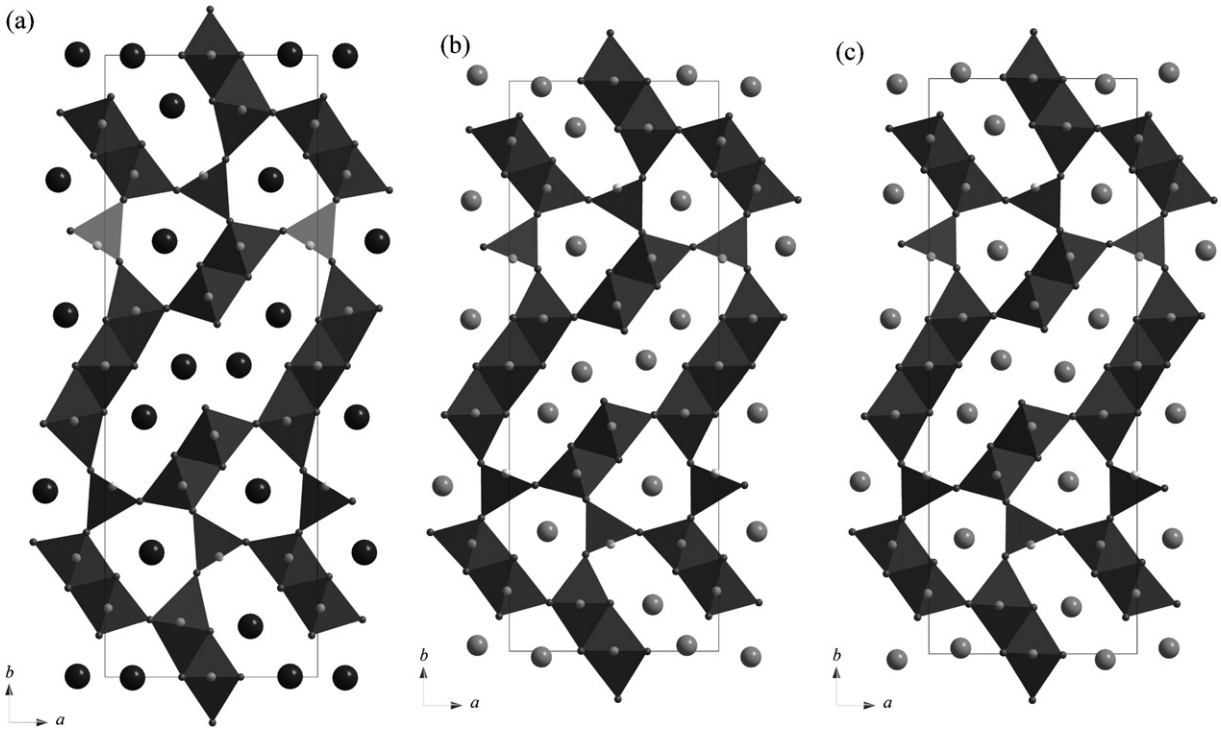

Fig. 4. Crystal structures of (a) $Na_{0.44}MnO_2$, (b) $Li_{0.44}MnO_2$, and (c) $Li_{0.55}MnO_2$.

analysis. The crystal structure of $Na_{0.44}MnO_2$ consists of double and triple rutile-type chains of edge-sharing MnO_6 octahedra and a single chain of edge-sharing MnO_5 that shares vertices, producing a framework containing large and small tunnels along the *c*-axis direction, with three types of Na ions located in the tunnels [2,6]. From a structural viewpoint, the MnO_5 coordination, as shown using triangles in Fig. 4, is not suitable for the electrochemical insertion/extraction reaction because in many cases, the five-coordinated Mn^{3+} cations could not change to Mn^{4+} upon delithiation. The additional Mn–O distance in $Na_{0.44}MnO_2$ was determined to be 3.19 Å from the result of the Rietveld analysis; this distance is too long for bonding. On the other hand, the sixth Mn–O distance decreased to 2.59 Å in $Li_{0.44}MnO_2$ and to 2.63 Å in $Li_{0.55}MnO_2$. These values are close to the reported Mn^{3+}–O distance, e.g., 2.409 Å in $NaMnO_2$ [9]. These results may suggest that all of the Mn sites are octahedrally coordinated in these lithium ion-exchanged samples, maintaining the original $Na_{0.44}MnO_2$-type framework structure.

The difference in the local structures between $Li_{0.44}MnO_2$ and $Li_{0.55}MnO_2$ is clearly ascertained based on the shape of the large tunnel space (Fig. 4). The expanded and distorted tunnel shape observed in $Na_{0.44}MnO_2$ and $Li_{0.44}MnO_2$ has been changed to a condensed and simple double-rectangular one in $Li_{0.55}MnO_2$. This structural change may cause a rearrangement of the lithium atoms in the tunnel space. Namely, the positions of the Li atoms in $Li_{0.44}MnO_2$ are the same those of the Na sites in $Na_{0.44}MnO_2$ [2], however, this oxygen-coordination environment around the Li atoms is too large for the lithium site. Unfortunately, the precise positions of the Li atoms in $Li_{0.55}MnO_2$ could not be refined in the present XRD study. The detailed crystal structure with an accurate lithium occupation in the tunnel spaces are currently being examined using neutron diffraction data and will be reported in a subsequent paper.

3.3. Electrochemical properties

Figs. 5–8 show the charge/discharge curves of the present $Li_{0.44+x}Mn_{1-y}Ti_yO_2$ samples starting from charging in the voltage range between 2.5 and 4.8 V, with a fixed current density of 30 mA g^{-1} (*C*/6) at 30 °C. Both the charge and discharge capacities were improved by the lithium-insertion treatments for these compounds, in comparison with those of the as-prepared $Li_{0.44}Mn_{1-y}Ti_yO_2$ compounds measured at a similar current density (30 mA g^{-1}). The initial charge capacity increased from

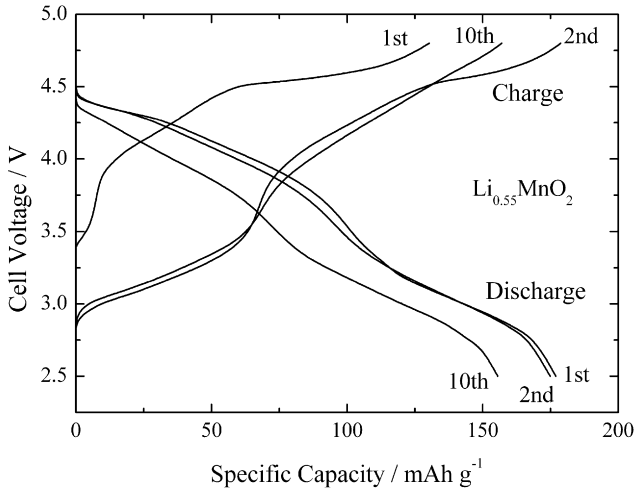

Fig. 5. Charge and discharge curves for the Li/$Li_{0.55}MnO_2$ cell.

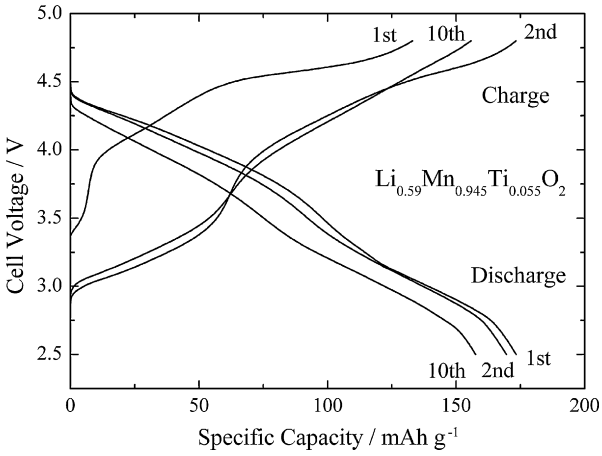

Fig. 6. Charge and discharge curves for the Li/$Li_{0.59}Mn_{0.945}Ti_{0.055}O_2$ cell.

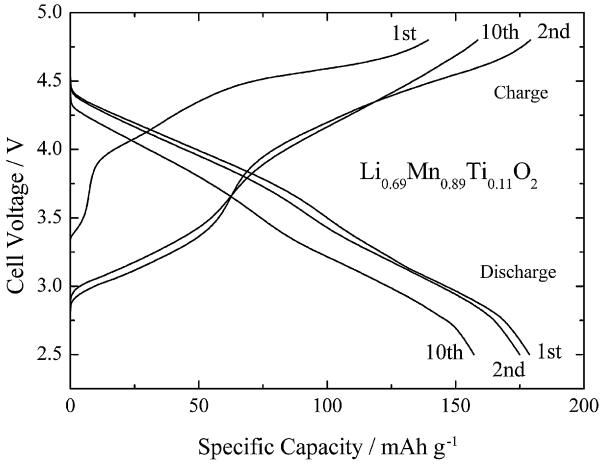

Fig. 7. Charge and discharge curves for the Li/$Li_{0.69}Mn_{0.89}Ti_{0.11}O_2$ cell.

130 mAh g^{-1} ($y = 0$) to 145 mAh g^{-1} ($y = 0.22$) together with the Ti content in these compounds. This fact is very consistent with the results of the chemical analysis for the lithium-inserted samples (Table 1). In addition, the initial discharge capacity improved together with the Ti content, as shown in

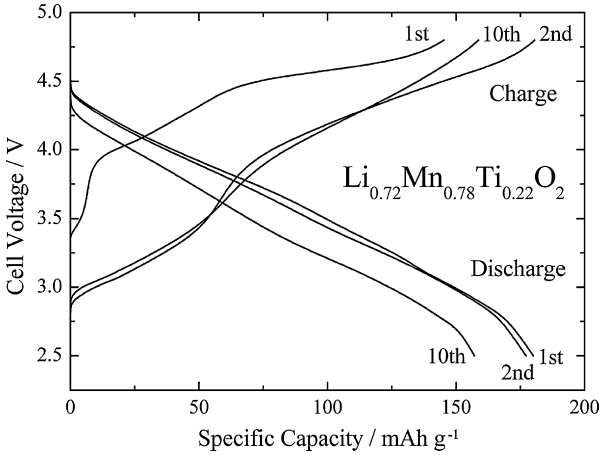

Fig. 8. Charge and discharge curves for the Li/$Li_{0.72}Mn_{0.78}Ti_{0.22}O_2$ cell.

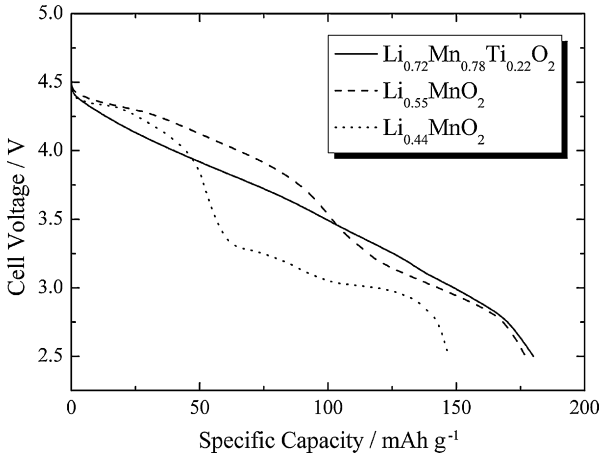

Fig. 9. Initial discharge curves for the Li/$Li_{0.44}MnO_2$, Li/$Li_{0.55}MnO_2$ and Li/$Li_{0.72}Mn_{0.78}Ti_{0.22}O_2$ cells.

Figs. 5–8. The maximum discharge capacity that was achieved was 180 mAh g^{-1} in the case of $Li_{0.72}Mn_{0.78}Ti_{0.22}O_2$. Above this substitution level ($y = 0.22$), the discharge capacity gradually decreased as the Ti content increased, as in the case of $Li_{0.44}Mn_{1-y}Ti_yO_2$ [5]. Furthermore, the discharge curve also changed shape from a profile with two distinct plateaus (Fig. 5) to a gradually sloping profile (Fig. 8) as the Ti content increased. Even after ten charge/discharge cycles, the capacity remained at 155 mAh g^{-1}, indicating an excellent cycling performance for these cells.

The initial discharge curves after charging up to 4.8 V for the Li/$Li_{0.44}MnO_2$, Li/$Li_{0.55}MnO_2$, and Li/$Li_{0.72}Mn_{0.78}Ti_{0.22}O_2$ cells are compared in Fig. 9. The initial discharge capacity was successfully improved by the lithium-insertion treatment from 146 mAh g^{-1} in the Li/$Li_{0.44}MnO_2$ cell to 177 mAh g^{-1} in the Li/$Li_{0.55}MnO_2$ cell. The discharge capacity at the 4 V plateau region in the lithium-inserted $Li_{0.55}MnO_2$ (about 100 mAh g^{-1}) was improved to twice that in the as-prepared $Li_{0.44}MnO_2$ (about 50 mAh g^{-1}).

Fig. 10 shows the XRD profile for the $Li_{0.55}MnO_2$ electrode after the above-mentioned electrochemical cycling experiment. No new peaks that suggest a spinel structure appear in this figure, and the pattern is very similar to that of the original

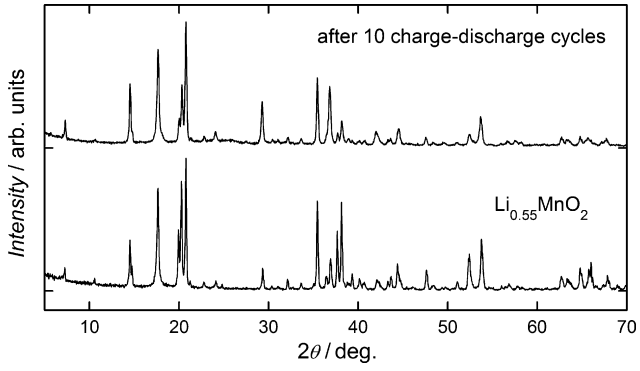

Fig. 10. XRD profiles of the sample after 10 charge/discharge cycles, and the initial $Li_{0.55}MnO_2$ as a reference.

$Li_{0.55}MnO_2$, indicating that the original tunnel structure (Fig. 4) is retained after the electrochemical charge/discharge cycling. From these facts, the improvement of the discharge capacity around 4 V in $Li_{0.55}MnO_2$ may be explained by the above-mentioned local structural change in the tunnel space together with the reconstruction of the Li occupations. Furthermore, the XRD measurements after the electrochemical experiments reveal that the original tunnel structure remains unchanged for all the $Li_{0.44+x}Mn_{1-y}Ti_yO_2$ electrodes in the present study.

4. Conclusions

The electrochemical performance of $Li_{0.44}Mn_{1-y}Ti_yO_2$ with the $Na_{0.44}MnO_2$-type tunnel structure was successfully improved by an additional lithium-insertion treatment using molten $LiNO_3$–LiOH salt at 270 °C. The discharge capacity at the 4 V plateau region in the lithium-inserted $Li_{0.55}MnO_2$ was improved to twice that in the as-prepared $Li_{0.44}MnO_2$, accompanying a local structural change in the tunnel shape. The Li/$Li_{0.44+x}Mn_{1-y}Ti_yO_2$ cells exhibited good charge/discharge performances with initial discharge capacities of 173–180 mAh g^{-1} between 2.5 and 4.8 V. In particular, a gradually sloping profile of the discharge curve between 2.5 and 4.8 V was revealed for the Li/$Li_{0.72}Mn_{0.78}Ti_{0.22}O_2$ cell. These facts indicate that the present lithium manganese oxides with the tunnel structure are promising candidates as future high-voltage positive electrodes for practical applications such as in electric vehicles (EVs).

Acknowledgments

We express our gratitude for the financial support from The New Energy and Industrial Technology Development Organization (NEDO) and Ministry of Economy, Trade and Industry (METI) in “Development of lithium battery technology for use by fuel cell vehicles, FY2002-FY2006.”

References

[1] M.M. Doeff, M.Y. Peng, Y. Ma, L.C. De Jonghe, J. Electrochem. Soc. 141 (1994) L145–L147.
[2] A.R. Armstrong, H. Huang, R.A. Jennings, P.G. Bruce, J. Mater. Chem. 8 (1998) 255–259.
[3] Y.U. Jeong, A. Manthiram, Electrochem. Solid State Lett. 2 (1999) 421–424.
[4] M.M. Doeff, T.J. Richardson, K.-T. Hwang, J. Power Sources 135 (2004) 240–248.
[5] J. Akimoto, J. Awaka, Y. Takahashi, N. Kijima, M. Tabuchi, A. Nakashima, H. Sakaebe, K. Tatsumi, Electrochem. Solid State Lett. 8 (2005) A554–A557.
[6] W.G. Mumme, Acta Crystallogr. Sect. B 24 (1968) 1114–1120.
[7] J.-P. Parant, R. Olazcuaga, M. Devalette, C. Fouassier, P. Hagenmuller, J. Solid State Chem. 3 (1971) 1–11.
[8] F. Izumi, T. Ikeda, Mater. Sci. Forum 321–324 (2000) 198–203.
[9] R. Hoppe, G. Brachtel, M. Jansen, Z. Anorg. Allgem. Chem. 417 (1975) 1–10.